Numerical simulation of nanorod growth in $REBa_2Cu_3O_y$ superconducting thin films

Yusuke Ichino (一野 祐亮), and Yutaka Yoshida (吉田 隆)

***Abstract*—Various nanostructures consisting of $BaMO_3$ (BMO) self-organize in $REBa_2Cu_3O_y$ (REBCO) films prepared by vapor phase epitaxy. A numerical simulation of the BMO self-organization was developed using the three-dimensional Monte Carlo (3D-MC) method, and the effects of deposition parameters such as substrate temperature (T_s), deposition rate (v_{dep}) and BMO volume fraction (f_{BMO}) on BMO self-organization were investigated. We consider only the kinetic factors and ignore mismatch strain on the nanorods morphology. 3D-MC simulations for various T_s indicated that the number density of BMO nanorods (NRs) decreased with an increase in T_s, and this tendency was similar to previous experimental results for $BaHfO_3$-doped SmBCO films prepared by the pulsed laser deposition method. The effects of v_{dep} and f_{BMO} were also simulated to provide contour plots of the number density of NRs with respect to T_s and f_{BMO} at various v_{dep}. Phase diagrams of nanostructures consisting of BMO with various v_{dep} were also obtained. Although these results do not take into account degradation of the superconducting properties and crystalline defects induced by non-optimized conditions, they are considered to be a useful guideline for control of the flux pinning landscape on REBCO coated conductors.**

***Index Terms*— Barium-metal complex oxides, Crystal growth simulation, Nanorods, $REBa_2Cu_3O_y$ thin films**

I. Introduction

Some barium-metal-complex oxides (BMOs) form diverse nanostructures in $REBa_2Cu_3O_y$ (REBCO; RE=Y, Sm, Gd etc.) superconducting thin films prepared by vapor phase epitaxy such as the pulsed laser deposition (PLD) and chemical vapor deposition (CVD) methods. MacManus-Driscoll et al. reported $BaZrO_3$ (BZO) *nanoparticles* (NPs) embedded in a YBCO film, the presence of which significantly improved the critical current density in a magnetic field [1]. Some other groups have confirmed the growth of BZO *nanorods* (NRs) in YBCO films [2-4]. Maiorov and colleagues showed that two types of flux pinning centers, randomly distributed NPs and columnar NRs, could be controlled by changing the substrate temperature or growth rate [5]. Our group has also reported that number density of BHO NRs can be controlled by changing the BHO volume fraction [6]. The same tendency has been reported even in BZO-doped YBCO films [4]. These reports clearly indicate that the BMO nanostructures are strongly affected by their deposition conditions.

Mele et al. reported that the superconducting properties of $BaSnO_3$ (BSO)-doped YBCO films, such as the critical temperature (T_c) and critical current density (J_c) in magnetic fields were affected by the BSO volume fraction [7]. We have recently reported on the superconducting properties of SmBCO films containing $BaHfO_3$ (BHO) NRs, of which the number density and morphology were dependent on the substrate temperature [8]. In particular, a BHO-doped SmBCO film deposited at 720 °C exhibited a macroscopic flux pinning force density of 1.6 TN/m^3 at 4.2 K, which is one of the highest values reported to date. In addition, the magnetic field angular dependence of J_c at 40 K for this sample was isotropically improved due to the discontinuous- and inclined-BHO NRs. These observations reveal that the number density and morphology of BMO nanostructures are very important for improving the superconducting properties in magnetic fields.

There have been some reports that have clarified the self-organization mechanism of BMO nanostructures. Wu et al. applied an elastic strain model between BZO NRs and a YBCO matrix to understand the effect of lattice strain on the diameter of the BZO NRs [4]. Our group developed a two-dimensional Monte Carlo (2D-MC) simulation code to elucidate the initial crystal growth stage of a two-component-system that corresponds to the BMO and REBCO system [9]. However, actual BMO nanostructures have only been observed using transmission electron microscopy (TEM); therefore, there have been no systematic reports on the effects of deposition parameters such as the substrate temperature (T_s), deposition rate (v_{dep}) and BMO volume fraction (f_{BMO}) on the number density and morphology of these nanostructures, although they play an important role in improvement of the superconducting properties. Therefore, we have developed a three-dimensional MC (3D-MC) simulation code to clarify the effect of the deposition parameters on the nanostructures without an experimental approach. Here, BMO nanostructures were systematically calculated under various deposition parameters to construct a phase diagram of the nanostructure morphologies. In this simulations, we consider only the kinetic factors and ignore mismatch strain on the nanorods morphology.

II. Simulation Method

A simple model was used, as shown in Fig. 1. A REBCO unit cell is represented as an *A* particle, which consists of three cubes, and a BMO unit cell is represented as one cube. The cubes have a side length of a = 0.4 nm. In an actual system, these lengths are different for each material, which leads to dislocations and strain around the interface of REBCO and BMO. However, in this simulation model, we did not take

This work was supported by JSPS KAKENHI Grant Numbers 15H04252, 15K14301, 15K14302 and 16H04512.

Y. Ichino and Y. Yoshida are with Dept. of Energy Engineering and Science, Nagoya University, Furo-cho, Chikusa-ku Nagoya 464-8603 Japan (e-mail: ichino@nuee.nagoya-u.ac.jp; yoshida@nuee.nagoya-u.ac.jp).

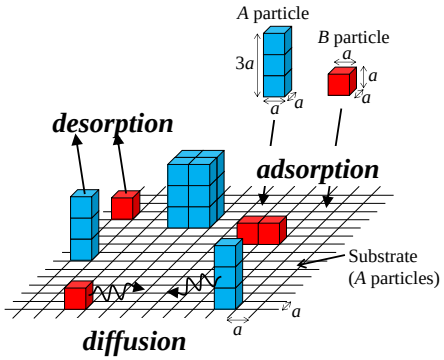

Fig. 1. Monte Carlo events occur on a substrate surface. Two types of particles are used in this model. The substrate consists of *A* particles.

such dislocations into account, and the strain energy was imposed through an interfacial bond energy between an *A* particle and a *B* particle, which is described in the following paragraph.

It was assumed that the substrate is constructed of *A* particles. The particles adsorb on the substrate from the vapor phase. There are no chemical reactions on the surface and the particles are allowed to move only to a nearest-neighbor site. The *A* particles always maintain a stacked structure perpendicular to the substrate surface, which corresponds to *c*-axis orientation in the REBCO thin films. Although *a*-axis grains arise at low substrate temperatures in an actual system, the *a*-axis grain growth was not taken into account in this model. The substrate area is 200×200 cubic grids, which corresponds to 80×80 nm^2 in physical units. Periodic boundary conditions were imposed on all the in-plane directions. f_{BMO} can be changed by varying the number ratio of adsorbed particles.

3D-MC simulations based on the standard Metropolis algorithm were conducted as follows. In a randomly selected point of the substrate sites, one of three possible events (adsorption, surface diffusion and desorption) can randomly occur. The frequency of adsorption (r_{ads}) and surface diffusion (r_{diff}) on a single surface site are denoted by $r_{ads} = Fa^2$ and $r_{diff} = D/a^2$, respectively. Here, *F* and *D* are the incident flux and surface diffusion constants, respectively. The growth kinetics of the film crystal are controlled by the dimensionless ratio *R*, where $R = r_{ads}/r_{diff}$. The *D* values used in this study were those reported by Dam et al., which were estimated from the surface morphologies of YBCO films with respect to the substrate temperature [10]. Using v_{dep}, *F* is expressed as $F = v_{dep}/(3a^3)$; therefore, v_{dep} has an influence on *R* through *F*.

The initial coordination energy (E_i) before a random walk and the final coordination energy (E_f) after the random walk were calculated. If $\Delta E = E_f - E_i$ is less than 0, then the particle moves preferentially to the final state. On the other hand, if ΔE_f is larger than 0, then the probability to move to the final state is defined by the Boltzmann distribution of $\exp(-\Delta E/k_B T)$, where k_B is the Boltzmann constant. The coordination energy is calculated by counting the interparticle bond energies. The bond energies were 2,000 K between *A* particles, 2,500 K between *B* particles and 500 K between *A* and *B* particles. This low bond energy between *A* and *B* particles indicates an unstable interface between these particles. The instability is caused by lattice strain. Lattice strain propagates in the whole REBCO matrix in an actual system; however, such propagation was not taken into account in this simulation.

The energy difference between an adsorbed particle and a particle in the vapor phase was 50,000 K. These energies were selected from preliminary simulations, whereby estimation could reproduce an actual number density of the BHO NRs in a BHO-doped SmBCO film prepared by conventional PLD method at T_s of 1,213 K [11]. The number density was measured from TEM observations.

T_s, v_{dep} and f_{BMO} were the simulation parameters examined here, and the morphologies of the nanostructures with respect to these parameters were evaluated. T_s, v_{dep} and f_{BMO} were varied from 1,023 to 1,193 K, from 10 to 3,000 nm/h, and from 0 to 30 vol.%, respectively.

III. Results and Discussion

A. *Effects of Deposition Conditions*

The T_s dependence of nanostructures consisting of *B* particles was calculated first. Figures 2(a) and 2(b) represent the nanostructures formed at T_s = 1,023 and 1,193 K, where v_{dep} and f_{BMO} were fixed at 70 nm/h and 3 vol.%, respectively. The *B* particles form NRs at both T_s. At the lower T_s, inclined-NRs are observed, whereas straight-NRs are formed at the higher T_s of 1,193 K. The number density of NRs becomes large at the lower T_s, so that many NRs arise and the growth rate decreases in the surface normal direction. The vertical growth of NRs is disturbed by the surrounding layers consisting of *A* particles; therefore, the growth of inclined-NRs in the film is preferential. The average inclination angle of the inclined-NRs was approximately 7.5°. At the higher T_s,

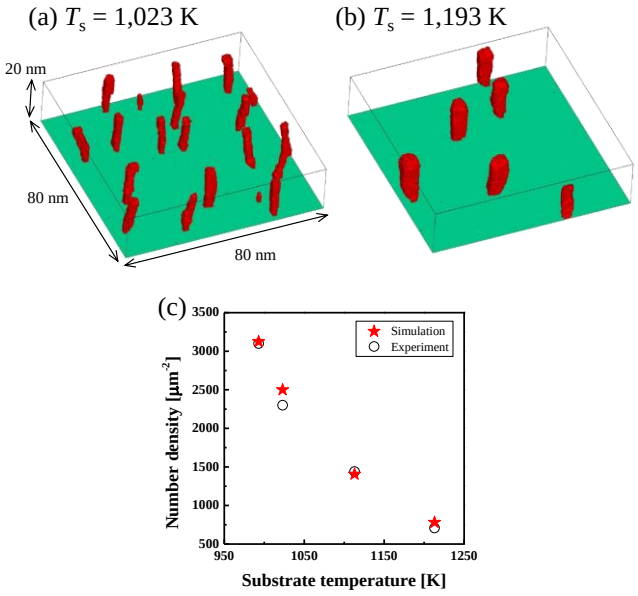

Fig. 2. Nanorod morphologies consisting of *B* particles at substrate temperatures of (a) 1,023 and (b) 1,193 K. The *A* particles are transparent and the *B* particles are colored red. The deposition rate and volume fraction of the *B* particles were 70 nm/h and 3 vol.%, respectively. (c) Number densities obtained from the simulations are compared with experimental results [8,11-13].

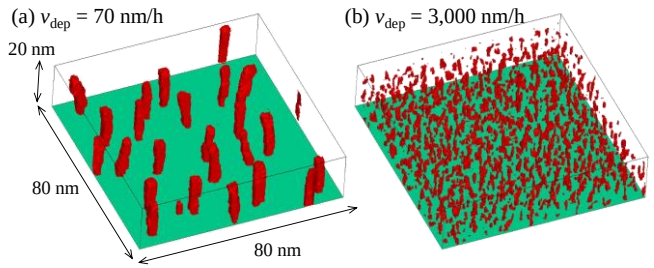

Fig. 3. Nanorod morphologies consisting of *B* particles for deposition rates of (a) 70 and (b) 3,000 nm/h. The *A* particles are transparent and the *B* particles are colored red. The substrate temperature and the volume fraction of *B* particles were 1,023 K and 5 vol.%, respectively.

the number density of NRs becomes small and the NR diameter increases compared with that at the lower T_s.

These tendencies are similar to our previous experimental results, where BHO-doped-SmBCO films were prepared at different T_s using the PLD method [12]. The number density of NRs was compared with experimental results confirmed by cross-sectional TEM observations [8,11-13], and the results are shown in Fig. 2(c). The T_s dependence of the experimental results is consistent with the 3D-MC simulation, and the number density was determined to decrease with an increase in T_s. Nucleation of the NRs is affected by supersaturation of the *B* particles on the substrate surface, and the supersaturation becomes lower with an increase in T_s. As a result, the number of nuclei consisting of *B* particles decreases, and the number density of the NRs decreases, while the diameters of the NRs increases due to a sufficient quantity of *B* particles for a single NR. In the case of the lower T_s, although the number density of the NRs was large, the amount of *B* particles supplied to a single NR was not sufficient, and a part of the single NR was covered by a matrix film layer consisting of *A* particles, which resulted in the formation of inclined-NRs.

The effect of v_{dep} on the nanostructure morphology was investigated, and the results are presented in Fig. 3. Here, v_{dep} = 70 nm/h was the typical deposition rate used experimentally, and 3,000 nm/h is a high deposition rate considering industrial production. T_s and f_{BMO} were fixed at 1,023 K and 5 vol.%, respectively. NRs were formed at low v_{dep}, whereas NR growth did not occur at high v_{dep}, but many NPs consisting of *B* particles were formed. The formation of NRs requires sufficient surface diffusion of *B* particles to reach a nucleus consisting of *B* particles. However, collisions between

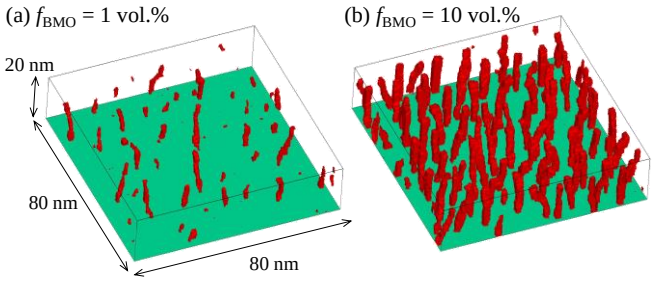

Fig. 4. Nanorod morphologies consisting of *B* particles at volume fractions of (a) 1 and (b) 10 vol.%. The *A* particles are transparent and the *B* particles are colored red. The substrate temperature and the deposition rate were 1,023 K and 300 nm/h, respectively.

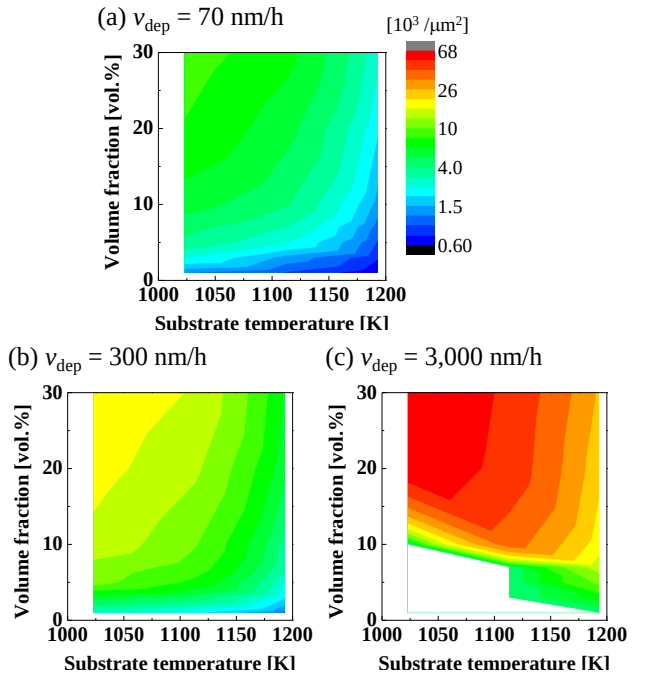

Fig. 5. Contour plots of nanorod number densities as a function of substrate temperature for various volume fractions of *B* particles at deposition rates of (a) 70, (b) 300, and (c) 3,000 nm/h.

particles on the surface increase at such high v_{dep}, and the diffusion length becomes short. As a result, the *B* particles cannot grow into NRs. Although the morphology of the NPs does not enhance J_c in magnetic fields applied parallel to the *c*-axis of REBCO films, the angular dependence of J_c under an applied magnetic field would be isotropically improved.

f_{BMO} also has an effect on the nanostructure morphology. Figure 4 shows the dependence of the nanostructure morphology on f_{BMO}. T_s and v_{dep} were fixed at 1,023 K and 300 nm/h, respectively. At low f_{BMO}, some inclined-NRs and NPs were formed, whereas high f_{BMO} resulted in a high number density of NRs and no NPs, because a sufficient amount of *B* particles to form NRs was supplied.

B. Phase Diagrams of Nanorod Morphologies

T_s, v_{dep} and f_{BMO} are correlated with each other in terms of the resultant nanostructure morphologies. Contour plots of the number density of NRs and phase diagrams of the nanostructures with respect to these parameters were constructed. Figure 5 shows contour plots of the NR number density as a function of T_s for various f_{BMO} with different v_{dep} of 70, 300, and 3,000 nm/h. At each v_{dep}, the number density of NRs increased with a decrease in T_s and with an increase in f_{BMO}. A high v_{dep} led to a high number density of NRs; at v_{dep} = 3,000 nm/h, the *B* particles could not grow into NRs at low T_s and low f_{BMO}, and the number density was not defined.

Diverse nanostructures that were dependent on the deposition parameters were formed. Phase diagrams of the nanostructures are summarized in Fig. 6. At a low v_{dep} of 70 nm/h, straight NRs or inclined-NRs were formed, as shown in Fig. 6(a). Sufficient surface diffusion was established with the low v_{dep}, so that NRs could be formed.

At v_{dep} = 300 nm/h, mixed nanostructures of short NRs and

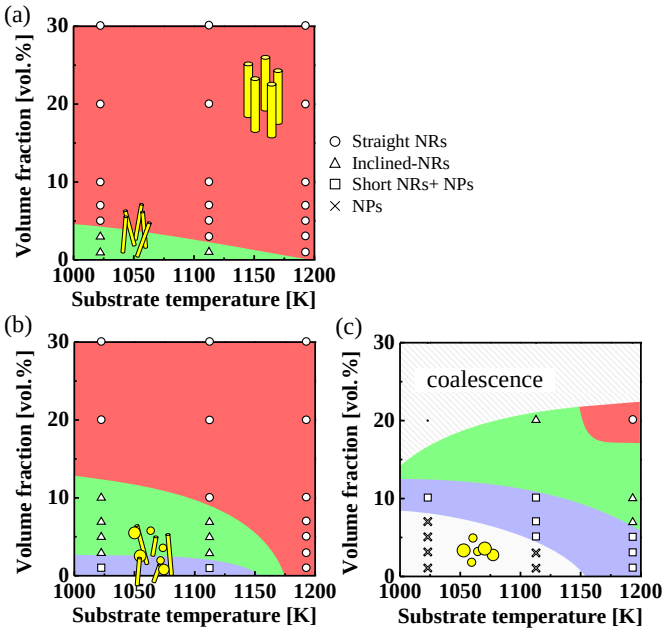

Fig. 6. Phase diagrams of the nanostructure morphologies as a function of substrate temperature for various volume fractions of *B* particles at deposition rates of (a) 70, (b) 300, and (c) 3,000 nm/h.

NPs were formed at low T_s and low f_{BMO}, as shown in Fig. 6(b). The surface diffusion lengths under these conditions decrease due to the higher v_{dep}, and some of the *B* particles would not grow into NR shapes. In addition, the region for the formation of inclined-NRs was expanded toward high f_{BMO}. A high v_{dep} leads to a greater number of nuclei consisting of *B* particles, which results in the formation of inclined-NRs due to an insufficient supply of *B* particles. This is similar to the case described in Fig. 2.

At v_{dep} = 3,000 nm/h, the region for the formation of inclined-NRs and that for short NRs + NPs move toward higher f_{BMO}, and the region for the formation of NPs appears at low T_s and low f_{BMO}, as shown in Fig. 6(c). The number density of NRs was very large for high f_{BMO} at approximately 30 vol.%, as shown in Fig. 6(c), so that the NRs coalesced.

Although these simulations do not take into account degradation of the superconducting properties and crystalline defects, such as *a*-axis grains and outgrowths induced by non-optimized conditions, these results are considered to be a useful guideline for control of the flux pinning landscape on REBCO coated conductors.

IV. Conclusion

3D-MC numerical simulations were performed for BMO self-organization in REBCO films with various deposition parameters such as substrate temperature, deposition rate and BMO volume fraction, and the resultant BMO nanostructure morphologies were evaluated with respect to these parameters. As the substrate temperature increased, the number density of the NRs decreased. The calculated number density was almost the same as our previous experimental results observed in $BaHfO_3$-doped SmBCO films prepared by PLD. At a high deposition rate, numerous nanoparticles appeared because of the short surface diffusion length due to frequent collisions between the particles. A low volume fraction of BMO resulted in insufficient nanostructure growth. These deposition parameters could thus be correlated with each other. Contour plots of NR number density and phase diagrams of the nanostructures were constructed with respect to the substrate temperature and volume fraction at various deposition rates. The contour plots and phase diagrams indicate that a high number density is achieved at lower substrate temperatures, higher volume fractions and higher deposition rates. However, the NRs coalesced at extremely high deposition rates and volume fractions. These results are expected to be useful for control of the flux pinning landscape for REBCO-coated conductors.

References

[1] J. L. MacManus-Driscoll, S. R. Foltyn, Q. X. Jia, H. Wang, A. Serquis, L. Civale, B. Maiorov, M. E. Hawley, M. P. Maley, and D. E. Peterson, "Strongly enhanced current densities in superconducting coated conductors of $YBa_2Cu_3O_{7-x}$ + $BaZrO_3$," *Nature Mater.*, vol. 3, p. 439, 2004.

[2] Y. Yamada, K. Takahashi, H. Kobayashi, M. Konishi, T. Watanabe, A. Ibi, T. Muroga, S. Miyata, T. Kato, T. Hirayama, and Y. Shiohara, "Epitaxial nanostructure and defects effective for pinning in $Y(RE)Ba_2Cu_3O_{7-x}$ coated conductors," *Appl. Phys. Lett.*, vol. 87, p. 132502, 2005.

[3] S. Kang, A. Goyal, J. Li, A. A. Gapud, P. M. Martin, L. Heatherly, J. R. Thompson, D. K. Christen, F. A. List, M. Paranthaman, and D. F. Lee, "High-performance high-T_c superconducting wires," *Science*, vol. 311, p. 1911, 2006.

[4] J. Z. Wu, J. J. Shi, J. F. Baca, R. Emergo, T. J. Haugan, B. Maiorov, and T. Holesinger, "The effect of lattice strain on the diameter of $BaZrO_3$ nanorods in epitaxial $YBa_2Cu_3O_{7-\delta}$ films," *Supercond. Sci. Technol.*, vol. 27, p. 044010, 2014.

[5] B. Maiorov, S. A. Baily, H. Zhou, O. Ugurlu, J. A. Kennison, P. C. Dowden, T. G. Holesinger, S. R. Foltyn, and L. Civale, "Synergetic combination of different types of defect to optimize pinning landscape using $BaZrO_3$-doped $YBa_2Cu_3O_7$," *Nature Mater.*, vol. 8, p. 398, 2009.

[6] S. Miura, Y. Yoshida, Y. Ichino, A. Tsuruta, K. Matsumoto, A. Ichinose, and S. Awaji, "Superconducting properties in $SmBa_2Cu_3O_y$ films with high density of $BaHfO_3$ nanorods fabricated with a seed layer," *IEEE Trans. Appl. Supercond.*, vol. 25, p. 6604904, 2015.

[7] P. Mele, K. Matsumoto, A. Ichinose, M. Mukaida, Y. Yoshida, S Horii, R. Kita, "Systematic study of the $BaSnO_3$ insertion effect on the properties of $YBa_2Cu_3O_{7-x}$ films prepared by pulsed laser ablation," *Supercond. Sci. Technol.*, vol. 21, 125017, 2008.

[8] S. Miura, Y. Yoshida, Y. Ichino, Q. Xu, K. Matsumoto, A. Ichinose, and S. Awaji, "Improvement in J_c performance below liquid nitrogen temperature for $SmBa_2Cu_3O_y$ superconducting films with $BaHfO_3$ nano-rods controlled by low-temperature growth," *APL Mater.*, vol. 4, p. 016102, 2016.

[9] Y. Ichino, A. Tsuruta, S. Miura, Y. Yoshida, M. Yoshizumi, and T. Izumi, "Determinant for self-organization of $BaMO_3$ nanorods included in vapor-phase-grown $REBa_2Cu_3O_y$ films," *IEEE Trans. Appl. Supercond.*, vol. 25, p. 6604506, 2015.

[10] B. Dam, J. H. Rector, J. M. Huijbregtse, and R. Griessen, "The transition from 2D-nucleation to spiral growth in pulsed laser deposited $YBa_2Cu_3O_{7-\delta}$ films," *Physica C*, vol. 305, p. 1, 1998.

[11] A. Tsuruta, Y. Yoshida, Y. Ichino, A. Ichinose, K. Matsumoto, and S. Awaji, "The influence of the geometric characteristics of nanorods on the flux pinning in high-performance $BaMO_3$-doped $SmBa_2Cu_3O_y$ films (M = Hf, Sn)," *Supercond. Sci. Technol.*, vol. 27, p. 065001, 2014.

[12] S. Miura, Y. Yoshida, Y. Ichino, A. Ichinose, K. Matsumoto, and S. Awaji, "Improvement of critical current densities in $SmBa_2Cu_3O_y$ films with $BaHfO_3$ nano-rods using low temperature growth technique," *J. Phys: Conference Series*, vol. 507, p. 022021, 2014.

[13] S. Miura, Y. Yoshida, Y. Ichino, K. Matsumoto, A. Ichinose, and S. Awaji, "Characteristics of high-performance $BaHfO_3$-doped $SmBa_2Cu_3O_y$ superconducting films fabricated with a seed layer and low temperature growth," *Supercond. Sci. Technol.*, vol. 28, p. 065013, 2015.